

# Renormalization of Einstein-Maxwell theory at one-loop

I. Y. Park

*†Department of Applied Mathematics, Philander Smith College  
Little Rock, AR 72223, USA  
inyongpark05@gmail.com*

## Abstract

Motivated by the recent foliation-based quantization scheme, we revisit the one-loop renormalization of an Einstein-Maxwell system. The systematic renormalization of the cosmological and Newton's constants is carried out by applying the refined background field method. The longstanding problem of the gauge choice-dependence of the effective action is addressed and the manner in which the gauge-choice independence is restored is discussed. The renormalization involves a metric field redefinition originally introduced by 't Hooft; with the field redefinition the theory is predictive.

# 1 Introduction

A gravitational system (see, e.g., [1–6] for reviews) is much subtler and more complex than a non-gravitational one in many ways. This aspect is manifest in various forms, most notably in the challenges in quantization, which in turn have been spawning various obstructions. One can easily name several areas in which a firmer grasp of the quantization would better position one for a more complete treatment. Any study, in particular, the study of black hole information, in which the back reaction of the metric plays (or is expected to play) an important role, should be an example. The cosmological constant problem is also likely to benefit since it is the vacuum energy the complete understanding of which must be accompanied by an account of its quantum shift. Much of the difficulty in the quantization must be attributed to the large amount of gauge symmetry, the diffeomorphism. Therefore, one can reasonably expect that the key to the puzzle should lie in proper handling of the gauge symmetry. It has recently been realized that the diffeomorphism symmetry can be tamed in a manner that accomplishes the long-sought renormalizability of gravity (in its physical sector) [7]. The renormalization procedures of pure Einstein gravity and an Einstein-scalar system have been carried out in [8–10] and [11, 12], respectively. We extend and expand those analyses to an Einstein-Maxwell system in this work.

The difficulties in a gravitational system could foster great opportunity, as, for instance, in holography, for understanding Nature. As is often the case (although nevertheless surprising if true), all these different aspects may not be unrelated and may well in fact hinge closely on one another. Our recent works on the gravity quantization were motivated by the black hole information. While working on the quantization, we have come to realize that our understanding of the boundary conditions and dynamics is as yet incomplete; a more systematic and sound analysis of the boundary conditions needs precede [13–16]<sup>1</sup> a complete treatment of the quantization. We have raised the possibility that information may be bleached through a quantum gravitational process in the vicinity of the horizon and released before the entry of the matter into the horizon [18] [19]. The cosmological constant is generically generated by the loop effects [12], as will be reviewed below, and

---

<sup>1</sup>As far as we are aware, its seriousness and importance have not, up until recently, been accordingly stressed. (See the recent work by Witten, [17] for a discussion of the boundary conditions.)

contributes to the generation of time-dependent solutions that in turn are linked with the black hole information [16].

The divergence analysis of an Einstein-Maxwell system was carried out long ago in an extensive work by Deser and van Nieuwenhuizen [20]. The counter-terms to the ultraviolet divergences were determined essentially by dimensional analysis and covariance. In our approach they are directly calculated in the Feynman diagrammatic method, with the results complementing their work in several aspects. We will also see, as a byproduct, how the long-known gauge dependence issue [21–25] arises and is cleared up (at least) in the present framework.

The case analysis of an Einstein-Maxwell system carries several more imminent significances for our perspective. Firstly, the matter part itself is a gauge system and this poses additional hurdles; overcoming them should constitute meaningful progress in the field. Secondly, it is in this work where the field redefinition-utilized renormalization program is more thoroughly carried out: the focus of [12] was on establishing the *renormalizability* of a gravity-matter system. A detailed and explicit analysis of, e.g., the running of the coupling constants was not conducted. In this work, the running of the cosmological constant and Newton’s constant is addressed in much detail. Since the renormalization involves a field redefinition, which is not necessary in the usual renormalizable theories, the explicit steps of the renormalization will be worth presenting - all of the required steps are taken in the present work. Further, the predictability of the theory - brought along by the renormalizability - is also explicitly addressed.

The paper is organized as follows.

In section 2, we outline the one-loop renormalization procedure in a general background metric  $g_{\mu\nu}$  that denotes a solution of the metric field equation. The analysis should make it clear that the methodology can be applied to an arbitrary background  $g_{\mu\nu}$ . The first several relatively simple diagrams and their relevant vertices are identified. In section 3, we carry out the explicit one-loop counter-term computation by taking  $g_{\mu\nu} = \eta_{\mu\nu}$ . A certain diagram yields a non-covariant expression and its inspection leads to a connection with the long-known problem of the gauge choice-dependence of the effective action. The gauge choice-dependence is then resolved. The origin of the gauge choice-dependence is found in the limitation of the background field

method (BFM), which can alternatively be viewed as a reflection of the complexity of a gravitational system. In section 4 we consider renormalization of the cosmological constant and Newton’s constant. The vacuum-to-vacuum and tadpole diagrams are responsible for their renormalization. Unlike in a non-gravitational theory, the tadpole diagrams play a potentially important role. There are several technical subtleties, some of which have to do with dimensional regularization: the flat propagator yields vanishing results for the vacuum-to-vacuum and tadpole diagrams. The shifts in the cosmological and Newton’s constants are introduced through finite renormalization. We show that the original Einstein-Hilbert action with the counter-terms can be rewritten as another Einstein-Hilbert action in terms of a redefined metric. Several ramifications including the theory’s predictability are discussed. Section 5 contains a summary and future directions. We contemplate on the several possible procedures of renormalization. We also comment on the higher-loop extension of the present work.

## 2 Loop computation setup

The preliminary step for renormalization is to compute the one-particle-irreducible (1PI) effective action in the given background. (See, e.g., [26] [27] [3] [28] for reviews of various methods of computing the effective action.) In this section, we lay broader outlines of the counter-term computation in an arbitrary background  $g_{\mu\nu}$  before getting into the flat case in the next section. We will focus on several two-point amplitudes.

Let us consider the Einstein-Maxwell action,<sup>2</sup>

$$S = \int \sqrt{-\hat{g}} \left( \frac{1}{\kappa^2} \hat{R} - \frac{1}{4} \hat{F}_{\mu\nu}^2 \right) \quad (2)$$

For the perturbative analysis in the background field method (BFM), introduce the fluctuation fields,  $(h_{\mu\nu}, a_\mu)$ , according to

$$\hat{g}_{\mu\nu} \equiv h_{\mu\nu} + \tilde{g}_{\mu\nu} \quad , \quad \hat{A}_\mu \equiv a_\mu + \tilde{A}_\mu \quad (3)$$

---

<sup>2</sup>To carry out renormalization, one starts with the renormalized form of the action:

$$S = \int \sqrt{-\hat{g}_r} \left( \frac{1}{\kappa_r^2} \hat{R}_r - \frac{1}{4} \hat{F}_{r\mu\nu}^2 \right) \quad (1)$$

where the renormalized quantities are indicated by the subscript  $r$  that has been omitted in (2) for simplicity of notation.

The graviton propagator associated with the traceless fluctuation mode [7, 9, 10] (see also [29])) can be written as

$$\langle h_{\mu\nu}(x_1)h_{\rho\sigma}(x_2) \rangle = \tilde{P}_{\mu\nu\rho\sigma} \tilde{\Delta}(x_1 - x_2) \quad (4)$$

where the tensor  $\tilde{P}_{\mu\nu\rho\sigma}$  is given by

$$\tilde{P}_{\mu\nu\rho\sigma} \equiv \frac{(2\kappa^2)}{2} \left( \tilde{g}_{\mu\rho}\tilde{g}_{\nu\sigma} + \tilde{g}_{\mu\sigma}\tilde{g}_{B\nu\rho} - \frac{1}{2}\tilde{g}_{\mu\nu}\tilde{g}_{\rho\sigma} \right); \quad (5)$$

$\tilde{\Delta}(x_1 - x_2)$  is the Green's function for a scalar theory in the background metric  $\tilde{g}_{\mu\nu}$ . (There is of course the full propagator for the vector field; we will focus on the graviton sector.) It turns out that it is convenient to employ two different layers of perturbation. As we will see, it is possible to formally construct  $\tilde{\Delta}(x_1 - x_2)$  in a closed-form; one may compute some of the diagrams by employing the full propagator (4) (as well as the full propagator of the Maxwell sector) - which we call the “first-layer” perturbation. For other diagrams such as the vacuum-to-vacuum amplitudes, one may employ the “second-layer” perturbation<sup>3</sup> by splitting  $\tilde{g}, \tilde{A}_\mu$  into

$$\tilde{g}_{\mu\nu} \equiv \varphi_{\mu\nu} + g_{\mu\nu} \quad , \quad \tilde{A}_\mu \equiv A_\mu + A_{0\mu} \quad (6)$$

where  $\varphi_{\mu\nu}, A_\mu$  represents the background fields and  $g_{\mu\nu}, A_{0\mu}$  the classical solutions. (For instance, we will take  $g_{\mu\nu} = \eta_{\mu\nu}, A_{0\mu} = 0$  in section 3.) For most of the diagrams that we will consider, the structures of the vertices allow one to approximate  $\tilde{P}_{\mu\nu\rho\sigma}$ , for the given order

$$\tilde{P}_{\mu\nu\rho\sigma} \simeq P_{\mu\nu\rho\sigma} \equiv \frac{(2\kappa^2)}{2} \left( g_{\mu\rho}g_{\nu\sigma} + g_{\mu\sigma}g_{\nu\rho} - \frac{1}{2}g_{\mu\nu}g_{\rho\sigma} \right) \quad (7)$$

where  $P_{\mu\nu\rho\sigma}$  is the leading-order  $\varphi_{\mu\nu}$ -expansion of  $\tilde{P}_{\mu\nu\rho\sigma}$ . (We will also see the use of the full tensor  $\tilde{P}_{\mu\nu\rho\sigma}$  in one of the computations, the first-layer perturbation example.) For the divergence analysis one can use  $\tilde{\Delta}(x_1 - x_2) \simeq \Delta(x_1 - x_2)$  where  $\Delta(x_1 - x_2)$  denotes the scalar propagator for  $g_{\mu\nu} = \eta_{\mu\nu}$ ,

$$\Delta(x_1 - x_2) = \int \frac{d^4k}{(2\pi)^4} \frac{e^{ik \cdot (x_1 - x_2)}}{ik^2} \quad (8)$$

In this “bottom-up” approach, the quantities that one intends to calculate in the first-layer perturbation can be calculated through the second-layer

---

<sup>3</sup>The second-layer perturbation is not necessary in non-gravitational theories.

perturbation. Dimensional analysis and 4D covariance provide useful consistency checks as will be demonstrated in section 3.

Let us expand the action in terms of the fluctuation fields  $h_{\mu\nu}, a_\mu$ . Including the gauge-fixing and ghost terms, one gets

$$S = \int \left( \frac{1}{\kappa^2} \mathcal{L}_{grav} + \mathcal{L}_{matter} \right) \quad (9)$$

where<sup>4</sup>

$$\begin{aligned} \kappa^2 \mathcal{L}_{grav} = & \frac{1}{2} \sqrt{-\tilde{g}} \left( -\frac{1}{2} \tilde{\nabla}_\gamma h^{\alpha\beta} \tilde{\nabla}^\gamma h_{\alpha\beta} + \frac{1}{4} \tilde{\nabla}_\gamma h_\alpha^\alpha \tilde{\nabla}^\gamma h_\beta^\beta \right. \\ & + h_{\alpha\beta} h_{\gamma\delta} \tilde{R}^{\alpha\gamma\beta\delta} - h_{\alpha\beta} h^\beta_\gamma \tilde{R}^{\kappa\alpha\gamma}_\kappa - h^\alpha_\alpha h_{\beta\gamma} \tilde{R}^{\beta\gamma} - \frac{1}{2} h^{\alpha\beta} h_{\alpha\beta} \tilde{R} + \frac{1}{4} h_\alpha^\alpha h_\beta^\beta \tilde{R} + \dots \Big) \\ & - \tilde{\nabla}^\nu \bar{C}^\mu \tilde{\nabla}_\nu C_\mu + \tilde{R}_{\mu\nu} \bar{C}^\mu C^\nu - \omega^* \tilde{\nabla}^\mu \tilde{F}_{\mu\nu} C^\nu - \omega^* \tilde{F}_{\mu\nu} \tilde{\nabla}^\mu C^\nu + \dots \end{aligned} \quad (10)$$

and

$$\begin{aligned} \mathcal{L}_{matter} = & -\frac{1}{4} \sqrt{-\tilde{g}} \left[ \tilde{g}^{\mu\nu} \tilde{g}^{\rho\sigma} - \tilde{g}^{\mu\nu} h^{\rho\sigma} - \tilde{g}^{\rho\sigma} h^{\mu\nu} + \frac{1}{2} \tilde{g}^{\mu\nu} \tilde{g}^{\rho\sigma} h + \tilde{g}^{\mu\nu} h^{\rho\kappa} h_\kappa^\sigma + \tilde{g}^{\rho\sigma} h^{\mu\kappa} h_\kappa^\nu \right. \\ & - \frac{1}{2} \tilde{g}^{\mu\nu} h h^{\rho\sigma} - \frac{1}{2} \tilde{g}^{\rho\sigma} h h^{\mu\nu} + h^{\mu\nu} h^{\rho\sigma} + \frac{1}{8} \tilde{g}^{\mu\nu} \tilde{g}^{\rho\sigma} (h^2 - 2h_{\kappa_1\kappa_2} h^{\kappa_1\kappa_2}) \Big] \left( f_{\mu\rho} f_{\nu\sigma} + 2f_{\mu\rho} \tilde{F}_{\nu\sigma} + \tilde{F}_{\mu\rho} \tilde{F}_{\nu\sigma} \right) \\ & - \frac{1}{2} \sqrt{-\tilde{g}} (\tilde{\nabla}_\kappa a^\kappa)^2 - \tilde{\nabla} \omega^* \tilde{\nabla} \omega + \dots \end{aligned} \quad (11)$$

where the raising and lowering are done by  $\tilde{g}^{\mu\nu}$  and  $\tilde{g}_{\mu\nu}$ , respectively. Above,  $(C^\kappa, \omega)$  are the ghosts for the diffeomorphism and vector gauge transformation, respectively.<sup>5</sup> Putting it all together, (9) can be written in a more useful form as the sum of the kinetic part and the vertices:

$$S \equiv S_k + S_v \quad (13)$$

---

<sup>4</sup>The  $\tilde{R}_{\mu\nu} \bar{C}^\mu C^\nu$  term of the gravity sector action  $\mathcal{L}_{grav}$  presented in [12] has a sign error due to mixed conventions. It, with affected equations, has been corrected in [9].

<sup>5</sup>These ghost terms correspond to the following transformations of the fluctuation fields [20]:

$$\begin{aligned} h'_{\mu\nu} &= h_{\mu\nu} + (\tilde{g}_{\mu\kappa} \tilde{D}_\nu + \tilde{g}_{\nu\kappa} \tilde{D}_\mu) \eta^\kappa + (h_{\mu\kappa} \tilde{D}_\nu + h_{\nu\kappa} \tilde{D}_\mu) \eta^\kappa + \eta^\kappa \tilde{D}_\kappa h^{\mu\nu} \\ a'_\mu &= a_\mu + \eta^\kappa \tilde{F}_{\kappa\mu} + \tilde{D}_\mu \eta^5 + a_\kappa \tilde{D}_\mu \eta^\mu + \eta^\kappa \tilde{D}_\kappa a_\mu \end{aligned} \quad (12)$$

under  $x'^\alpha = x^\alpha - \eta^\alpha$  and the vector gauge transformation with the parameter  $-\eta^\kappa \tilde{A}_\kappa + \eta^5$ .

with

$$\begin{aligned}
S_k = & \int \sqrt{-\tilde{g}} \frac{1}{2\kappa^2} \left( -\frac{1}{2} \tilde{\nabla}_\gamma h^{\alpha\beta} \tilde{\nabla}^\gamma h_{\alpha\beta} + \frac{1}{4} \tilde{\nabla}_\gamma h_\alpha^\alpha \tilde{\nabla}^\gamma h_\beta^\beta \right) - \frac{1}{4} \sqrt{-\tilde{g}} \left( \tilde{g}^{\mu\nu} \tilde{g}^{\rho\sigma} f_{\mu\rho} f_{\nu\sigma} \right) \\
& - \frac{1}{2} \sqrt{-\tilde{g}} (\tilde{\nabla}_\kappa a^\kappa)^2 + \frac{1}{2\kappa^2} \sqrt{-\tilde{g}} (-\tilde{\nabla}^\nu \bar{C}^\mu \tilde{\nabla}_\nu C_\mu) - \sqrt{-\tilde{g}} \tilde{\nabla}^\rho \omega^* \tilde{\nabla}_\rho \omega \quad (14)
\end{aligned}$$

and

$$\begin{aligned}
S_v = & \int \sqrt{-\tilde{g}} \frac{1}{2\kappa^2} \left( h_{\alpha\beta} h_{\gamma\delta} \tilde{R}^{\alpha\gamma\beta\delta} - h_{\alpha\beta} h^\beta_\gamma \tilde{R}^{\kappa\alpha\gamma}_\kappa - h^\alpha_\alpha h_{\beta\gamma} \tilde{R}^{\beta\gamma} - \frac{1}{2} h^{\alpha\beta} h_{\alpha\beta} \tilde{R} \right. \\
& + \frac{1}{4} h^\alpha_\alpha h^\beta_\beta \tilde{R} \left. \right) - \frac{1}{4} \sqrt{-\tilde{g}} (\tilde{g}^{\mu\nu} \tilde{g}^{\rho\sigma}) \left( +2f_{\mu\rho} \tilde{F}_{\nu\sigma} + \tilde{F}_{\mu\rho} \tilde{F}_{\nu\sigma} \right) - \frac{1}{4} \sqrt{-\tilde{g}} \left[ -\tilde{g}^{\mu\nu} h^{\rho\sigma} \right. \\
& - \tilde{g}^{\rho\sigma} h^{\mu\nu} + \frac{1}{2} \tilde{g}^{\mu\nu} \tilde{g}^{\rho\sigma} h + \tilde{g}^{\mu\nu} h^{\rho\kappa} h_\kappa^\sigma + \tilde{g}^{\rho\sigma} h^{\mu\kappa} h_\kappa^\nu - \frac{1}{2} \tilde{g}^{\mu\nu} h h^{\rho\sigma} - \frac{1}{2} \tilde{g}^{\rho\sigma} h h^{\mu\nu} \\
& + h^{\mu\nu} h^{\rho\sigma} + \frac{1}{8} \tilde{g}^{\mu\nu} \tilde{g}^{\rho\sigma} (h^2 - 2h_{\kappa_1\kappa_2} h^{\kappa_1\kappa_2}) \left. \right] \left( f_{\mu\rho} f_{\nu\sigma} + 2f_{\mu\rho} \tilde{F}_{\nu\sigma} + \tilde{F}_{\mu\rho} \tilde{F}_{\nu\sigma} \right) \\
& + \frac{1}{2\kappa^2} \sqrt{-\tilde{g}} \left( +\tilde{R}_{\mu\nu} \bar{C}^\mu C^\nu + \frac{1}{2} \tilde{\nabla}^\mu \omega^* \tilde{F}_{\mu\nu} C^\nu \right) + \dots \quad (15)
\end{aligned}$$

## 2.1 on the gauge-fixing

A crucial feature of the action above - which has been set up for the refined BFM - is how the graviton gauge-fixing has been implemented:

$$-\frac{1}{2} \left[ \tilde{\nabla}_\nu h^{\mu\nu} - \frac{1}{2} \tilde{\nabla}^\mu h \right]^2 \quad (16)$$

This is the refined BFM version of the usual gauge-fixing,

$$-\frac{1}{2} \left[ \nabla_\nu h^{\mu\nu} - \frac{1}{2} \nabla^\mu h \right]^2 \quad (17)$$

that is  $\tilde{g}_{\mu\nu}$ -background non-covariant. In other words, one starts with (17) and converts it into (16) when turning to the refined BFM. The physical content of the gauge condition satisfied by  $h_{\mu\nu}$  is still (17) since the BFM is just a convenience device that allows one to conduct the analysis more covariantly than otherwise. (The field  $\varphi_{\mu\nu}$  satisfies the same gauge-fixing; see (51) below.) Naively, one expects that with the gauge-fixing (16) the 1PI effective action will come out to be  $\tilde{g}_{\mu\nu}$ -covariant. Later we will see that the 1PI action is non-covariant due to the presence of the terms that can be

removed by enforcing the strong form of the gauge condition, which provides an important clue as to how to solve the gauge choice-dependence of the effective action.

## 2.2 two-point diagrams

In general the renormalization in a curved background  $g_{\mu\nu}$  is technically involved. It is nevertheless possible to outline the steps of the amplitude computation for an arbitrary solution metric  $g_{\mu\nu}$ .

Cautionary remarks are in order. It is important to distinguish the second-layer diagrams from the first-layer ones. Only the first-layer diagrams will individually yield covariant results. A given first-layer diagram corresponds, in general, to multiple second-layer diagrams even at a fixed order of  $\varphi_{\mu\nu}$ . Consider, for example, the graviton kinetic action,

$$\mathcal{L}_{grav,kin} = \frac{1}{2\kappa^2} \sqrt{-\tilde{g}} \left( -\frac{1}{2} \tilde{\nabla}_\gamma h^{\alpha\beta} \tilde{\nabla}^\gamma h_{\alpha\beta} + \frac{1}{4} \tilde{\nabla}_\gamma h_\alpha^\alpha \tilde{\nabla}^\gamma h_\beta^\beta \right) \quad (18)$$

and the one-loop vacuum-to-vacuum amplitude. Although there is a unique one-loop vacuum-to-vacuum amplitude, , in the first-layer perturbation, the diagram corresponds to multiple second-layer ones. At the second order in  $\varphi_{\alpha\beta}$ , the relevant diagram is the one given in Fig. 1 (a). More on this as we continue.

With the split given in (6), the kinetic terms themselves yield the vertices for the second-layer perturbation expansion. For instance, the graviton kinetic term is expanded as

$$\begin{aligned} 2\kappa^2 \mathcal{L}_{grav,kin} = & -\frac{1}{2} \partial_\gamma h^{\alpha\beta} \partial^\gamma h_{\alpha\beta} + \frac{1}{4} \partial_\gamma h_\alpha^\alpha \partial^\gamma h_\beta^\beta \\ & + \left( 2g^{\beta\beta'} \tilde{\Gamma}^{\alpha'\gamma\alpha} - g^{\alpha\beta} \tilde{\Gamma}^{\alpha'\gamma\beta'} \right) \partial_\gamma h_{\alpha\beta} h_{\alpha'\beta'} + \left[ \frac{1}{2} (g^{\alpha\alpha'} g^{\beta\beta'} \varphi^{\gamma\gamma'} + g^{\beta\beta'} g^{\gamma\gamma'} \varphi^{\alpha\alpha'} \right. \\ & \left. + g^{\alpha\alpha'} g^{\gamma\gamma'} \varphi^{\beta\beta'} \right) - \frac{1}{4} \varphi g^{\alpha\alpha'} g^{\beta\beta'} g^{\gamma\gamma'} - \frac{1}{2} g^{\gamma\gamma'} g^{\alpha'\beta'} \varphi^{\alpha\beta} + \frac{1}{4} (-\varphi^{\gamma\gamma'} + \frac{1}{2} \varphi g^{\gamma\gamma'}) g^{\alpha\beta} g^{\alpha'\beta'} \left. \right] \partial_\gamma h_{\alpha\beta} \partial_{\gamma'} h_{\alpha'\beta'} \end{aligned} \quad (19)$$

where the raising and lowering are done by  $g^{\mu\nu}$  and  $g_{\mu\nu}$ , respectively. The terms in the second and third lines serve as the vertices responsible for Fig. 1 (a). The corresponding ghost diagram is given in Fig. 1 (b). The forms of all possible second-layer vertices can be obtained by applying this scheme

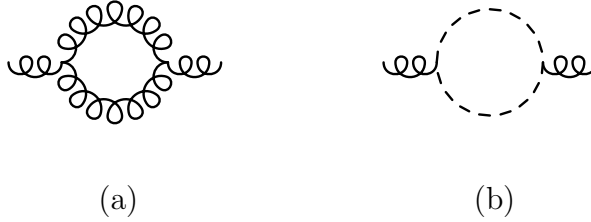


Figure 1: graviton and ghost diagrams (indices on fields suppressed)

to the rest of the terms in eq. (14) and (15). The first several relatively simple matter-involving diagrams are listed in Fig. 2. In general, we restrict the maximum number of the graviton external lines to two for simplicity. Overall, the diagrams are classified into four categories. The first class is the diagrams with both vertices from the graviton sector: the pure gravity sector two-point amplitude and the corresponding ghost-loop diagram in Fig. 1. They were considered in [9] and will be reviewed below. The second is the diagrams with both vertices from the matter sector, Fig. 2 (a) and (c). The third is the diagrams with one vertex from the graviton sector and the other from the matter sector, Fig. 2 (d).

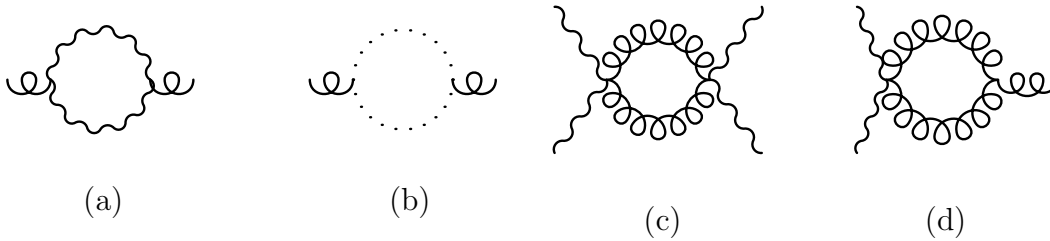


Figure 2: matter-involving diagrams

All of the diagrams so far have “homogeneous” loops whereas the diagrams in Fig. 3 have “inhomogeneous” ones. They are classified as the fourth class due to the fact that they require special care.

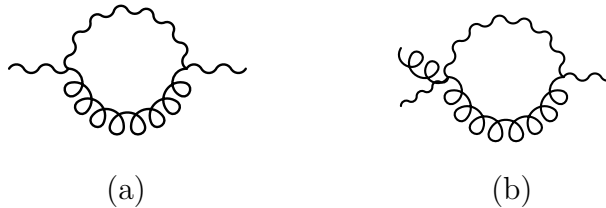


Figure 3: diagrams with inhomogeneous loops

The vertex,  $V_g$ , responsible for the diagrams in Fig. 1 (a), is defined by rewriting (19) as

$$\mathcal{L} = \frac{1}{\kappa'^2} \left[ -\frac{1}{2} \partial_\gamma h^{\alpha\beta} \partial^\gamma h_{\alpha\beta} + \frac{1}{4} \partial_\gamma h_\alpha^\alpha \partial^\gamma h_\beta^\beta + \mathcal{L}_{V_{g1}} \right] \quad (20)$$

where

$$\kappa'^2 \equiv 2\kappa^2 \quad (21)$$

and

$$\begin{aligned} V_g \equiv & \sqrt{-g} \left( 2g^{\beta\beta'} \tilde{\Gamma}^{\alpha'\gamma\alpha} - g^{\alpha\beta} \tilde{\Gamma}^{\alpha'\gamma\beta'} \right) \partial_\gamma h_{\alpha\beta} h_{\alpha'\beta'} + \sqrt{-g} \left[ \frac{1}{2} (g^{\alpha\alpha'} g^{\beta\beta'} \varphi^{\gamma\gamma'} + g^{\beta\beta'} g^{\gamma\gamma'} \varphi^{\alpha\alpha'} \right. \\ & + g^{\alpha\alpha'} g^{\gamma\gamma'} \varphi^{\beta\beta'}) - \frac{1}{4} \varphi g^{\alpha\alpha'} g^{\beta\beta'} g^{\gamma\gamma'} - \frac{1}{2} g^{\gamma\gamma'} g^{\alpha'\beta'} \varphi^{\alpha\beta} + \frac{1}{4} (-\varphi^{\gamma\gamma'} + \frac{1}{2} \varphi g^{\gamma\gamma'}) g^{\alpha\beta} g^{\alpha'\beta'} \left. \right] \partial_\gamma h_{\alpha\beta} \partial_{\gamma'} h_{\alpha'\beta'} \\ & + \sqrt{-\tilde{g}} \left( h_{\alpha\beta} h_{\gamma\delta} \tilde{R}^{\alpha\gamma\beta\delta} - h_{\alpha\beta} h_\gamma^\beta \tilde{R}^{\kappa\alpha\gamma}{}_\kappa - h_\alpha^\alpha h_{\beta\gamma} \tilde{R}^{\beta\gamma} - \frac{1}{2} h^{\alpha\beta} h_{\alpha\beta} \tilde{R} + \frac{1}{4} h_\alpha^\alpha h_\beta^\beta \tilde{R} \right) \end{aligned} \quad (22)$$

As for  $\tilde{g}_{\mu\nu}$ -containing quantities, expansion in terms of  $\varphi_{\mu\nu}$  is to be understood. The vertex responsible for the ghost-loop diagram can be similarly identified by expanding the terms quadratic in the ghost field:

$$\begin{aligned} V_C \equiv & - \left[ \frac{1}{2} \varphi \partial^\mu \bar{C}^\nu \partial_\mu C_\nu - \tilde{\Gamma}_{\mu\nu}^\lambda (\partial^\mu \bar{C}^\nu C_\lambda - \partial^\mu C^\nu \bar{C}_\lambda) \right. \\ & \left. - (g^{\nu\beta} \varphi^{\mu\alpha} + g^{\mu\alpha} \varphi^{\nu\beta}) \partial_\beta \bar{C}_\alpha \partial_\nu C_\mu \right] + R_{\mu\nu} \bar{C}^\mu C^\nu \end{aligned} \quad (23)$$

The vertices responsible for the diagrams in Fig. 2 and Fig. 3 can be similarly obtained by examining the matter part of the action (the trace piece  $h \equiv \tilde{g}^{\alpha\beta} h_{\alpha\beta}$  has been set to zero [7, 9, 10]:

$$\begin{aligned} V_{m1} & \equiv -\frac{1}{4} \sqrt{-g} \left[ -g^{\rho\sigma} \varphi^{\mu\nu} - g^{\mu\nu} \varphi^{\rho\sigma} \right] f_{\mu\rho} f_{\nu\sigma} \\ V_{m2} & \equiv -\frac{1}{4} \sqrt{-g} \left[ g^{\mu\nu} h^{\rho\kappa} h_\kappa^\sigma + g^{\rho\sigma} h^{\mu\kappa} h_\kappa^\nu + h^{\mu\nu} h^{\rho\sigma} - \frac{1}{4} g^{\mu\nu} g^{\rho\sigma} h_{\kappa_1\kappa_2} h^{\kappa_1\kappa_2} \right] \tilde{F}_{\mu\rho} \tilde{F}_{\nu\sigma} \\ V_{m3} & \equiv \frac{1}{2} \sqrt{-g} \left[ g^{\mu\nu} h^{\rho\sigma} + g^{\rho\sigma} h^{\mu\nu} \right] f_{\mu\rho} F_{\nu\sigma} \\ V_{m4} & \equiv -\frac{1}{2} \sqrt{-g} \left[ \varphi^{\mu\nu} h^{\rho\sigma} + \varphi^{\rho\sigma} h^{\mu\nu} \right] f_{\mu\rho} F_{\nu\sigma} \end{aligned} \quad (24)$$

Let us work out the counter-terms to the diagrams in Fig. 1 to 3. Below

“  $\Rightarrow$  ” means that the diagram on the left-hand side leads to the counter-term(s) on the right-hand side

The graviton and ghost contributions respectively are

$$\text{Diagram 1} \Rightarrow -\frac{1}{2} \frac{1}{\kappa'^4} \left\langle \left( \int V_g \right)^2 \right\rangle \quad (25)$$

and

$$\text{Diagram 2} \Rightarrow -\frac{1}{2} \frac{1}{\kappa'^4} \left\langle \left( \int V_C \right)^2 \right\rangle \quad (26)$$

The numerical  $-\frac{1}{2}$  is the combinatoric factor that arises when the vertices are brought down from the exponent in the path integral. The total gravity sector one-loop counter-terms are given by the sum of these two; the result for the flat case was obtained in [9] will be quoted in section 3. The diagrams in Fig. 2 (a) and (c) have two vertices,  $V_{m1}$  and  $V_{m2}$ , inserted respectively. For the diagram in Fig. 2 (a) and (c) one gets

$$\text{Diagram 3} \Rightarrow -\frac{1}{2} \left\langle \left( \int V_{m1} \right)^2 \right\rangle = -\frac{1}{2} \left\langle \left[ \int \frac{1}{4} (g^{\rho\sigma} \varphi^{\mu\nu} + g^{\mu\nu} \varphi^{\rho\sigma}) (f_{\mu\rho} f_{\nu\sigma}) \right]^2 \right\rangle \quad (27)$$

$$\begin{aligned} \text{Diagram 4} \Rightarrow -\frac{1}{2} \left\langle \left( \int V_{m2} \right)^2 \right\rangle = -\frac{1}{2} \left\langle \left[ \int \frac{1}{4} (g^{\mu\nu} h^{\rho\kappa} h_\kappa^\sigma + g^{\rho\sigma} h^{\mu\kappa} h_\kappa^\nu + h^{\mu\nu} h^{\rho\sigma} \right. \right. \\ \left. \left. - \frac{1}{4} g^{\mu\nu} g^{\rho\sigma} h_{\kappa_1 \kappa_2} h^{\kappa_1 \kappa_2}) (\tilde{F}_{\mu\rho} \tilde{F}_{\nu\sigma}) \right]^2 \right\rangle \quad (28) \end{aligned}$$

The cross-term diagram in Fig. 2 (d) is generated by the vacuum expectation value of the two vertices, one of which is the matter vertex  $V_{m2}$  and the other  $V_g$ . The diagram corresponds to

$$\begin{aligned} \text{Diagram 5} \Rightarrow - \left\langle \int V_{m2} \int V_g \right\rangle = - \left\langle \int \left( -\frac{1}{4} \right) \left[ g^{\mu\nu} h^{\rho\kappa} h_\kappa^\sigma + g^{\rho\sigma} h^{\mu\kappa} h_\kappa^\nu + h^{\mu\nu} h^{\rho\sigma} \right. \right. \\ \left. \left. - \frac{1}{4} g^{\mu\nu} g^{\rho\sigma} h_{\kappa_1 \kappa_2} h^{\kappa_1 \kappa_2} \right] (\tilde{F}_{\mu\rho} \tilde{F}_{\nu\sigma}) \times \frac{1}{\kappa'^2} \int \left\{ \left( 2g^{\beta\beta'} \tilde{\Gamma}^{\alpha'\gamma\alpha} - g^{\alpha\beta} \tilde{\Gamma}^{\alpha'\gamma\beta'} \right) \partial_\gamma h_{\alpha\beta} h_{\alpha'\beta'} \right. \right. \\ \left. \left. + \left[ \frac{1}{2} (g^{\alpha\alpha'} g^{\beta\beta'} \varphi^{\gamma\gamma'} + g^{\beta\beta'} g^{\gamma\gamma'} \varphi^{\alpha\alpha'} + g^{\alpha\alpha'} g^{\gamma\gamma'} \varphi^{\beta\beta'}) - \frac{1}{2} g^{\gamma\gamma'} g^{\alpha'\beta'} \varphi^{\alpha\beta} \right. \right. \right. \\ \left. \left. \left. - \frac{1}{4} \varphi^{\gamma\gamma'} g^{\alpha\beta} g^{\alpha'\beta'} \right] \partial_\gamma h_{\alpha\beta} \partial_{\gamma'} h_{\alpha'\beta'} + \left( h_{\alpha\beta} h_{\gamma\delta} \tilde{R}^{\alpha\gamma\beta\delta} - h_{\alpha\beta} h_{\gamma\delta}^{\beta\gamma} \tilde{R}^{\kappa\alpha\gamma\kappa} - \frac{1}{2} h^{\alpha\beta} h_{\alpha\beta} \tilde{R} \right) \right\} \right\rangle \quad (29) \end{aligned}$$

The computation of the diagrams with the inhomogeneous loops serves as an example of the first-layer perturbation. For them it is necessary to use the full propagator in (4), a step not needed for the other diagrams so far for a structural reason. In the first-layer perturbation, the graph to calculate is



Figure 4: first-layer perturbation diagram

Note that unlike Fig. 3 (a), the lines have been thickened. The external lines represent the full fields, i.e., the fields with tildes. By the same token, the internal lines represent the full propagators. (The two diagrams in Fig. 3 are the first two terms that result from, so to speak,  $\varphi_{\alpha\beta}$ -expanding the graph in Fig. 4. There are additional contributions coming from the internal lines when the full propagators are used.) As for the diagrams in Fig. 3, they can be set up in a manner similar to the others:

$$\begin{aligned}
 \text{Diagram 1} &\Rightarrow -\frac{1}{2} \langle \left( \int V_{m3} \right)^2 \rangle = -\frac{1}{2} \langle \left( \int \frac{1}{2} (g^{\mu\nu} h^{\rho\sigma} + g^{\rho\sigma} h^{\mu\nu}) f_{\mu\rho} F_{\nu\sigma} \right)^2 \rangle \\
 \text{Diagram 2} &\Rightarrow - \langle \int V_{m3} \int V_{m4} \rangle = - \langle \int \frac{1}{2} (g^{\mu\nu} h^{\rho\sigma} + g^{\rho\sigma} h^{\mu\nu}) f_{\mu\rho} F_{\nu\sigma} \\
 &\quad \times \int \frac{-1}{2} (\varphi^{\mu'\nu'} h^{\rho'\sigma'} + \varphi^{\rho'\sigma'} h^{\mu'\nu'}) f_{\mu'\rho'} F_{\nu'\sigma'} \rangle \quad (30)
 \end{aligned}$$

We will leave it for now and come back in section 3 where we show a more convenient way of effectively calculating all the contributions, including those arising from the full internal propagators.

### 2.3 vacuum-to-vacuum and tadpole diagrams

In the first-layer perturbation, the shifts in the cosmological and Newton's constants are caused by the vacuum-to-vacuum and tadpole diagrams, respectively (more details in section 4). Fig. 5 lists the diagrams for the pure gravity sector; there are similar diagrams for the matter-involving sector. For

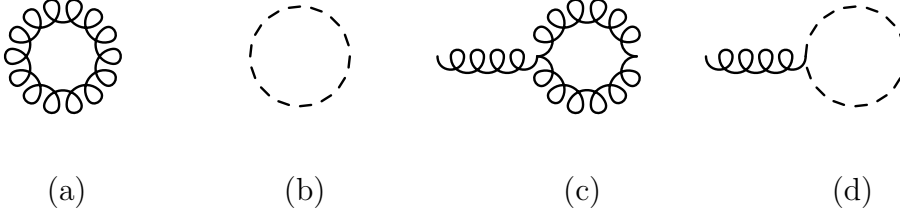


Figure 5: vacuum and tadpole diagrams

the graviton vacuum-to-vacuum amplitude, for example, one is to compute

$$\int \prod_x dh_{\kappa_1 \kappa_2} e^{\frac{i}{\kappa^2} \int \sqrt{-g} \left( -\frac{1}{2} \tilde{\nabla}_\gamma h^{\alpha\beta} \tilde{\nabla}^\gamma h_{\alpha\beta} \right)} \quad (31)$$

This vacuum energy amplitude in the first-layer perturbation will give a vacuum diagram and a tadpole diagram in the second-layer. These diagrams as well as the genuine tadpole diagrams will be analyzed in detail in section 4.

### 3 Flat space analysis

In this section we consider a flat background. The analysis can also be viewed as the computation of the divergences in a curved background: the flat space analysis captures them since the ultraviolet divergence is a short-distance phenomenon. In the past the counter-terms were determined by dimensional analysis and covariance [20]. We directly calculate them in the refined background field method; dimensional analysis and covariance play the *subsidiary* role of checking the results.

Let us consider a flat background

$$g_{\mu\nu} = \eta_{\mu\nu} \quad , \quad A_{0\mu} = 0 \quad (32)$$

with dimensional regularization. In what follows we will present the explicit flat spacetime computations for the two-point diagrams considered for a generic background  $g_{\mu\nu}$  in the previous section. Although the techniques of the counter-term computation themselves are similar to those used in the pure gravity [9] and gravity-scalar [12] analyses, the present case has several

additional complications. As an unexpected spin-off of our direct approach, we will see how the long-known gauge choice-dependence issue is resolved.

### 3.1 two-point diagrams

The pure gravity sector was analyzed in [9]. Consider the ghost loop diagram in Fig. 1 (b) first. The ghost vertex takes, in the flat spacetime,

$$V_C = - \left[ -\tilde{\Gamma}_{\mu\nu}^{\lambda} (-C_{\lambda} \partial^{\mu} \bar{C}^{\nu} + \bar{C}_{\lambda} \partial^{\mu} C^{\nu}) - (\eta^{\nu\beta} \varphi^{\mu\alpha} + \eta^{\mu\alpha} \varphi^{\nu\beta}) \partial_{\beta} \bar{C}_{\alpha} \partial_{\nu} C_{\mu} \right] + R_{\mu\nu} \bar{C}^{\mu} C^{\nu}$$

Let us define, for convenience,

$$V_C = V_{C,I} + V_{C,II} \quad (33)$$

with

$$\begin{aligned} V_{C,I} &\equiv - \left[ -\tilde{\Gamma}_{\mu\nu}^{\lambda} (-C_{\lambda} \partial^{\mu} \bar{C}^{\nu} + \bar{C}_{\lambda} \partial^{\mu} C^{\nu}) - (\eta^{\nu\beta} \varphi^{\mu\alpha} + \eta^{\mu\alpha} \varphi^{\nu\beta}) \partial_{\beta} \bar{C}_{\alpha} \partial_{\nu} C_{\mu} \right] \\ V_{C,II} &\equiv R_{\mu\nu} \bar{C}^{\mu} C^{\nu} \end{aligned} \quad (34)$$

The correlator to be computed is

$$\begin{aligned} -\frac{1}{2} \frac{1}{\kappa'^4} < \left( \int V_{C,I} + V_{C,II} \right)^2 > = -\frac{1}{2} \frac{1}{\kappa'^4} < \left\{ \int \left[ -\tilde{\Gamma}_{\mu\nu}^{\lambda} (\partial^{\mu} \bar{C}^{\nu} C_{\lambda} - \partial^{\mu} C^{\nu} \bar{C}_{\lambda}) \right. \right. \\ &\quad \left. \left. - (\eta^{\nu\beta} \varphi^{\mu\alpha} + \eta^{\mu\alpha} \varphi^{\nu\beta}) \partial_{\beta} \bar{C}_{\alpha} \partial_{\nu} C_{\mu} \right] - R_{\mu\nu} \bar{C}^{\mu} C^{\nu} \right\}^2 > \end{aligned} \quad (35)$$

To see how the dimensional analysis and covariance can be utilized to check the final results, consider, e.g.,  $< (\int V_{C,I})^2 >$ ; a direct calculation yields

$$\begin{aligned} &-\frac{1}{2} \frac{1}{\kappa'^4} < \left( \int V_{C,I} \right)^2 > \\ &= -\frac{1}{2} \frac{\Gamma(\epsilon)}{(4\pi)^2} \int \left[ -\frac{2}{15} \partial^2 \varphi_{\mu\nu} \partial^2 \varphi^{\mu\nu} + \frac{4}{15} \partial^2 \varphi^{\alpha\kappa} \partial_{\kappa} \partial_{\sigma} \varphi_{\alpha}^{\sigma} - \frac{1}{30} (\partial_{\alpha} \partial_{\beta} \varphi^{\alpha\beta})^2 \right] \end{aligned} \quad (36)$$

where the parameter  $\epsilon$  is related to the total spacetime dimension  $D$  by

$$D = 4 - 2\epsilon \quad (37)$$

The result above (and some of the present ones) were obtained with the help of the Mathematica package xAct'xTensor' in performing the index contractions. By invoking dimensional analysis and covariance, one expects the

result to come out to be a sum of  $R^2$  and  $R_{\mu\nu}^2$  to the second order of  $\varphi_{\rho\sigma}$  with appropriate coefficients. With the traceless condition  $\varphi = 0$  explicitly enforced,  $R^2$  and  $R_{\mu\nu}^2$  are given, to the second order in  $\varphi_{\alpha\beta}$ , by

$$\begin{aligned} R^2 &= \partial_\mu \partial_\nu \varphi^{\mu\nu} \partial_\rho \partial_\sigma \varphi^{\rho\sigma} \\ R_{\alpha\beta} R^{\alpha\beta} &= \frac{1}{4} \left[ \partial^2 \varphi^{\mu\nu} \partial^2 \varphi_{\mu\nu} - 2 \partial^2 \varphi^{\alpha\kappa} \partial_\kappa \partial_\sigma \varphi_\alpha^\sigma + 2 (\partial_\mu \partial_\nu \varphi^{\mu\nu})^2 \right]; \end{aligned} \quad (38)$$

from these it follows

$$-\frac{1}{2} \frac{1}{\kappa'^4} \left\langle \left( \int V_{C,I} \right)^2 \right\rangle = -\frac{1}{2} \frac{\Gamma(\epsilon)}{(4\pi)^2} \int \left[ -\frac{8}{15} \tilde{R}_{\alpha\beta} \tilde{R}^{\alpha\beta} + \frac{7}{30} \tilde{R}^2 \right] \quad (39)$$

The tildes on the fields in the counter-terms will be omitted from now on. Let us complete the other terms in (35); collecting all, one gets, for the ghost diagram,

$$\text{ghost loop} \Rightarrow -\frac{1}{2} \frac{\Gamma(\epsilon)}{(4\pi)^2} \int \left[ \frac{7}{15} R_{\mu\nu} R^{\mu\nu} + \frac{17}{30} R^2 \right] \quad (40)$$

As for the graviton-loop diagram in Fig. 1 (a), the vertex  $V_g$  takes

$$\begin{aligned} V_g \equiv & \left( 2\eta^{\beta\beta'} \tilde{\Gamma}^{\alpha'\gamma\alpha} - \eta^{\alpha\beta} \tilde{\Gamma}^{\alpha'\gamma\beta'} \right) \partial_\gamma h_{\alpha\beta} h_{\alpha'\beta'} + \left[ \frac{1}{2} (\eta^{\alpha\alpha'} \eta^{\beta\beta'} \varphi^{\gamma\gamma'} + \eta^{\beta\beta'} \eta^{\gamma\gamma'} \varphi^{\alpha\alpha'} \right. \\ & \left. + \eta^{\alpha\alpha'} \eta^{\gamma\gamma'} \varphi^{\beta\beta'} \right) - \frac{1}{2} \eta^{\gamma\gamma'} \eta^{\alpha'\beta'} \varphi^{\alpha\beta} - \frac{1}{4} \varphi^{\gamma\gamma'} \eta^{\alpha\beta} \eta^{\alpha'\beta'} \left] \partial_\gamma h_{\alpha\beta} \partial_{\gamma'} h_{\alpha'\beta'} \right. \\ & \left. + \left( h_{\alpha\beta} h_{\gamma\delta} \tilde{R}^{\alpha\gamma\beta\delta} - h_{\alpha\beta} h_\gamma^\beta \tilde{R}^{\kappa\alpha\gamma}_\kappa - \frac{1}{2} h^{\alpha\beta} h_{\alpha\beta} \tilde{R} \right) \right] \quad (41) \end{aligned}$$

By using the traceless propagator one can show:

$$\text{graviton loop} \Rightarrow -\frac{1}{2} \frac{\Gamma(\epsilon)}{(4\pi)^2} \int \left[ -\frac{23}{20} R_{\mu\nu} R^{\mu\nu} - \frac{23}{40} R^2 \right] \quad (42)$$

The correlators for the matter-involving sector have also been outlined in the previous section. Their flat spacetime evaluation leads to the following results for the diagrams in Fig. 2 (a)-(c):

$$\begin{aligned} \text{matter loop (a)} &\Rightarrow \frac{\Gamma(\epsilon)}{(4\pi)^2} \int \left( \frac{1}{30} R^2 - \frac{1}{10} R_{\alpha\beta} R^{\alpha\beta} \right) \\ \text{matter loop (b)} &\Rightarrow -\frac{\Gamma(\epsilon)}{(4\pi)^2} \frac{1}{15} \int R_{\alpha\beta} R^{\alpha\beta} \\ \text{matter loop (c)} &\Rightarrow \frac{\kappa'^4 \Gamma(\epsilon)}{(4\pi)^2} \frac{3}{64} \int (F_{\alpha\beta} F^{\alpha\beta})^2 \end{aligned} \quad (43)$$

These results are covariant as expected. The direct calculation of the diagram in Fig. 2 (d) yields

$$\text{Diagram} \Big|_{V_I+V_{II}} \Rightarrow \frac{\kappa'^2 \Gamma(\epsilon)}{(4\pi)^2} \int \left( \frac{1}{16} F_{\mu\nu} F^{\mu\nu} \partial_\alpha \partial_\beta \varphi^{\alpha\beta} + \frac{1}{2} F_{\mu\kappa} F_\nu{}^\kappa \partial^2 \varphi^{\mu\nu} \right) \quad (44)$$

which is non-covariant.<sup>6</sup> As a matter of fact, this is the diagram that suggests the solution for the gauge choice-dependence. This non-covariant result will be examined in section 3.2 and we will see how the covariance is restored. The diagram above also receives a contribution from  $V_{III}$  vertex:

$$\text{Diagram} \Big|_{V_{III}} \Rightarrow \frac{\kappa'^2 \Gamma(\epsilon)}{(4\pi)^2} \int \left( \frac{3}{4} F_{\alpha\kappa} F_\beta{}^\kappa R^{\alpha\beta} + \frac{1}{8} F_{\alpha\beta} F^{\alpha\beta} R \right. \\ \left. + \frac{1}{4} F_{\alpha\delta} F_{\beta\gamma} R^{\alpha\beta\gamma\delta} - \frac{1}{4} F_{\alpha\beta} F_{\gamma\delta} R^{\alpha\beta\gamma\delta} \right) \quad (45)$$

As for the diagrams with the inhomogeneous loops, the first-layer diagram to be computed is the one in Fig. 4. It corresponds to several second-layer diagrams, two of which are Fig. 3 (a) and (b); one can show

$$\text{Diagram} \Rightarrow \frac{\kappa'^2 \Gamma(\epsilon)}{2 (4\pi)^2} \int \left( \frac{1}{3} \partial_\alpha F^\alpha{}_\kappa \partial_\beta F^{\beta\kappa} - \frac{1}{12} \partial_\rho F_{\alpha\beta} \partial^\rho F^{\alpha\beta} \right) \\ \text{Diagram} \Rightarrow \kappa'^2 \frac{\Gamma(\epsilon)}{(4\pi)^2} \int \left( \frac{1}{3} F_{\alpha\kappa} \partial_\lambda \partial^\beta F_\beta{}^\kappa \varphi^{\alpha\lambda} - \frac{1}{12} F_{\alpha\kappa} \partial^2 F_\beta{}^\kappa \varphi^{\alpha\beta} \right) \quad (46)$$

where all of the index contractions are done with the flat metric. Whereas the first diagram is covariant at the leading order, the second diagram is not at its given order, the  $\varphi_{\alpha\beta}$ -linear order. There are also contributions arising from the higher-order internal propagators and all of these three different contributions are required for the covariance since they altogether correspond to the single first-layer diagram in Fig. 4. Keeping track of the higher-order internal propagators obviously requires the full (or at least higher-order) propagator expression  $\tilde{\Delta}$ . Therefore, instead of separately computing the individual contributions, it will be more economical to compute them at one

---

<sup>6</sup>In the case of the Einstein-scalar system analyzed in [12], we obtained a covariant result for a similar diagram, . The present non-covariant result is one reflection of the complexity of the gauge matter system.

stroke. The calculation can be done by performing the following steps: let us consider

$$\mathbf{V} \equiv \frac{1}{2} \left[ \tilde{g}^{\rho\sigma} h^{\mu\nu} + \tilde{g}^{\mu\nu} h^{\rho\sigma} \right] f_{\mu\rho} F_{\nu\sigma} \quad (47)$$

where  $\tilde{g}^{\mu\nu}$  is taken to be the linear-order expression,  $\tilde{g}^{\mu\nu} = g^{\mu\nu} - \varphi^{\mu\nu}$ ; the contractions are carried out by  $\tilde{g}_{\mu\nu}$ . At this point we introduce the orthonormal basis  $e_a^\mu$ :

$$\tilde{e}_a^\mu \tilde{e}_b^\nu \tilde{g}_{\mu\nu} = \eta_{ab} \quad (48)$$

where the Latin indices run  $a, b = 0, 1, 2, 3$ . The full scalar propagator  $\tilde{\Delta}$  can be written

$$\tilde{\Delta}(X_1 - X_2) = \int \frac{d^4 L}{(2\pi)^4} \frac{e^{iL_c(X_1 - X_2)^c}}{iL_a L_b \eta^{ab}} \quad (49)$$

where  $X^a$  and  $L_c$  are the coordinates and momenta associated with the orthonormal basis. Then the computation of the two-point amplitude goes identically with that of Fig. 3 (a); switching back to the original frame, one gets

$$\text{Diagram} \Rightarrow -\frac{1}{2} \langle \left( \int \mathbf{V} \right)^2 \rangle = \frac{\kappa'^2}{2} \frac{\Gamma(\epsilon)}{(4\pi)^2} \int \left( \frac{1}{3} \nabla_\alpha F^\alpha{}_\kappa \nabla_\beta F^{\beta\kappa} - \frac{1}{12} \nabla_\rho F_{\alpha\beta} \nabla^\rho F^{\alpha\beta} \right) \quad (50)$$

The analysis of the vacuum-to-vacuum amplitudes and tadpoles will be presented in section 4.

### 3.2 on gauge-choice independence

Above, we have evaluated the counter-terms for the diagrams in Figures. 1 to 5, and they have led to different types of the counter-terms, one of which, i.e., eq. (44), has come out non-covariant. This means that the effective action, as it stands, is non-covariant and gauge fixing-dependent. It turns out that these two problems have the following common solution: once the

gauge-fixing<sup>7</sup>

$$\partial_\mu \varphi^{\mu\nu} = 0 \quad (52)$$

is explicitly imposed on the effective action, the covariance and gauge-choice independence are restored.

To see this, let us examine the non-covariant counter-terms for Fig. 2 (c) given in (44). Note that the first term in (44) vanishes upon imposing the strong form of the gauge condition  $\partial_\mu \varphi^{\mu\nu} = 0$ , which implies<sup>8</sup>

$$\partial_\nu \partial_\mu \varphi^{\mu\nu} = 0; \quad (54)$$

with it eq. (44) now takes

$$\begin{array}{c} \text{Diagram: a circle of wavy lines} \\ \left|_{V_I + V_{II}} \right. \end{array} \Rightarrow \frac{\kappa'^2 \Gamma(\epsilon)}{(4\pi)^2} \int \left( \frac{1}{2} F_{\mu\kappa} F_\nu{}^\kappa \partial^2 \varphi^{\mu\nu} \right) = -\frac{\kappa'^2 \Gamma(\epsilon)}{(4\pi)^2} \int F_{\mu\kappa} F_\nu{}^\kappa R^{\mu\nu} \quad (55)$$

where the second equality is valid, as usual, up to a certain order of  $\varphi_{\alpha\beta}$ , the linear order for the present case. Note that above, the following identity at  $\varphi_{\rho\sigma}$ -linear order has been used:

$$R_{\mu\nu} = \frac{1}{2} (\partial^\kappa \partial_\mu \varphi_{\kappa\nu} + \partial^\kappa \partial_\nu \varphi_{\kappa\mu} - \partial_\mu \partial_\nu \varphi - \partial^2 \varphi_{\mu\nu}) = -\frac{1}{2} \partial^2 \varphi_{\mu\nu} \quad (56)$$

where the second equality results once the gauge conditions are enforced.

One is now in a position to address the longstanding issue of the gauge choice-dependence of the effective action: The effective action becomes fully covariant and gauge-choice independent after enforcing  $\partial_\nu \varphi^{\mu\nu} = 0$ . One

---

<sup>7</sup>Note that the gauge-fixing

$$\partial_\mu \varphi^{\mu\nu} - \partial^\nu \varphi = 0 \quad (51)$$

reduces to (52) once the traceless condition  $\varphi = 0$  is enforced.

<sup>8</sup>It is with the following caveat. Since the scalar curvature  $R$  is given by

$$R = \partial_\alpha \partial_\beta \varphi^{\alpha\beta} \quad (53)$$

to the linear order, it is not possible, with the strong form of the gauge condition, to probe the presence of the  $R$ -factor through the current linear-order calculation. For that, it is necessary to go to the second order.

should view the covariant action as still supplemented by the gauge-fixing. (This is just like the classical action: the classical action is fully covariant but is to be supplemented by a gauge-fixing condition.) If one chooses a different gauge-fixing and carries out the amplitude computations in that gauge, one should get exactly the same covariant effective action up to the terms that can be removed by that gauge-condition; this time, the action is supplemented with the very gauge-fixing condition that one has chosen. Therefore, the gauge-choice independence of the effective action should be interpreted to mean that the action is covariant after enforcing the strong form of the gauge condition and that the covariant action is to be supplemented by the gauge-fixing condition of one's choice. (But one can of course choose any gauge-fixing (namely even a gauge-fixing different from the initial one) once the covariant effective action is obtained.)

One may wonder whether the appearance of the factors of  $\partial_\mu\varphi^{\mu\nu}$  in the counter-term calculation of (44) could by any chance be made to disappear, say, without imposing the gauge condition. It appears that the gauge choice-dependence has a deeper root. To be specific, let us consider the proof of the gauge-choice independence in chap. 15 of [30]. The proof is for a gauge theory in the ordinary (i.e., non-BFM) path-integral. The gauge choice-dependence gets to reside in a field-independent constant (therein denoted by  $C$ ; see eq. (15.5.19)), which is then duly disregarded. If one employs the BFM, however, that constant comes to depend on the background fields (say,  $\varphi_{\mu\nu}$  for the present case, for example) and this must be the gauge choice-dependence that we have observed. This shows that the BFM, refined or not, has a limitation when applied to a gravitational system: it is introduced aiming for a more covariant treatment of the effective action computation. It turns out to be at odds with the gauge-choice independence.<sup>9</sup> The limitation is overcome by imposing the gauge condition in its strong form as we have just discussed.

---

<sup>9</sup>Nevertheless, the refined BFM has an advantage compared to the conventional BFM in that the latter would yield results non-covariant in an uncontrollable way whereas the former gives the results covariant up to the gauge-choice dependent terms that can be removed by enforcing the strong form of the gauge condition.

## 4 One-loop renormalization

The focus of the previous section was on the divergent parts of the diagrams; the analysis was involved but relatively straightforward. The forms of the counter-terms have been obtained with the infinite parts of the coefficients specified. As well known in the standard quantum field theory, one has the freedom to adjust the finite parts of the coefficients through the renormalization scheme, which one may take to be the modified minimal subtraction  $\overline{\text{MS}}$  (see, e.g., [31] for a review). The main focus of the present section is to carry out the renormalization in detail and study its implications.

For the detailed analysis involving the renormalization conditions, it is convenient, as commonly done, to introduce a scale parameter  $\mu$  by making the following shift:

$$\kappa^2 \rightarrow \mu^{-n/2+2} \kappa^2 \quad (57)$$

With this, eq.(1) takes

$$S = \int \sqrt{-\hat{g}} \left( \frac{1}{\kappa^2 \mu^{2-n/2}} \hat{R} - \frac{1}{4} \hat{F}_{\mu\nu}^2 \right) \quad (58)$$

One can proceed and compute various amplitudes and counter-terms; that was basically what we did in the previous section, but this time the parameter  $\mu$  will be included. The finite parts can now be kept track of with the fixed renormalization scheme.

One of the main goals of this section is to analyze the renormalization of the cosmological and Newton's constants (earlier works can be found, e.g., in [32–34]). In its entirety the procedure involves dealing with an infinite number of counter-terms, not just the cosmological constant and Einstein-Hilbert terms. It will be nevertheless useful to first hone in on the renormalization of those two constants, a task undertaken at the end of section 4.1 before working out the further details of the whole procedure in section 4.2. This is because these constants carry special physical meanings unlike the other newly appearing couplings that will ultimately be absorbed by a metric field redefinition. Moreover, there are some subtleties in the evaluation of the diagrams responsible for their renormalization.

Let us first frame the analysis of the vacuum and tadpole diagrams in preparation for section 4.1. The vacuum-to-vacuum amplitude Fig. 5 (a) takes the form of the cosmological constant term and diverges (see, e.g., in

[30] and [12]). (The discussion here is for a flat spacetime, but the divergence will be quite generically produced for an arbitrary background.) Thus if we were dealing with a massive theory it would take a counter-term of the form of the cosmological constant of an infinite value to remove the divergence. However, the vacuum energy diagram vanishes due to an identity (eq. (64) below) in dimensional regularization. This is a rather undesirable feature of dimensional regularization when dealing with a massless theory.<sup>10</sup> The diagrams responsible for the renormalization of the Newton's constant are the tadpole diagrams. As we will see in detail in section 4.1, the (would-be) shift in the Newton's constant is caused by a diagram that results from self-contraction of two fluctuation fields within the given vertex. Again, the following identity makes the regularization less suitable for the tadpole diagrams:

$$\int d^D k \frac{1}{(k^2)^\omega} = 0 \quad (59)$$

where  $\omega$  is an arbitrary number. The tadpole diagram vanishes due to this: the divergence that would otherwise renormalize the Newton's constant is taken to vanish. For the reasons to be explained, we will introduce the shifts in the cosmological and Newton's constants through finite renormalization.

## 4.1 vacuum-to-vacuum and tadpole diagrams

The kinetic terms are responsible for the vacuum-to-vacuum amplitudes in the parlance of the first-layer perturbation. We quote them here for convenience; this time it is written as

$$\begin{aligned} 2\kappa^2 \mathcal{L} &= \sqrt{-\tilde{g}} \left( -\frac{1}{2} \tilde{\nabla}_\gamma h^{\alpha\beta} \tilde{\nabla}^\gamma h_{\alpha\beta} + \frac{1}{4} \tilde{\nabla}_\gamma h_\alpha^\alpha \tilde{\nabla}^\gamma h_\beta^\beta \right) \\ &= -\frac{1}{2} \partial_\gamma h^{\alpha\beta} \partial^\gamma h_{\alpha\beta} + \frac{1}{4} \partial_\gamma h_\alpha^\alpha \partial^\gamma h_\beta^\beta + V_{g,I} + V_{g,II} \end{aligned} \quad (60)$$

---

<sup>10</sup>For instance, the identities in (59) and (64) often obscure cancellations between the bosonic and fermionic amplitudes in a supersymmetric field theory, making them separately vanish.

where

$$\begin{aligned}
V_{g,I} &\equiv \left( 2\eta^{\beta\beta'}\tilde{\Gamma}^{\alpha'\gamma\alpha} - \eta^{\alpha\beta}\tilde{\Gamma}^{\alpha'\gamma\beta'} \right) \partial_\gamma h_{\alpha\beta} h_{\alpha'\beta'} \\
V_{g,II} &\equiv \left[ \frac{1}{2}(\eta^{\alpha\alpha'}\eta^{\beta\beta'}\varphi^{\gamma\gamma'} + \eta^{\beta\beta'}\eta^{\gamma\gamma'}\varphi^{\alpha\alpha'} + \eta^{\alpha\alpha'}\eta^{\gamma\gamma'}\varphi^{\beta\beta'}) \right. \\
&\quad - \frac{1}{4}\varphi\eta^{\alpha\alpha'}\eta^{\beta\beta'}\eta^{\gamma\gamma'} - \frac{1}{2}\eta^{\gamma\gamma'}\eta^{\alpha'\beta'}\varphi^{\alpha\beta} \\
&\quad \left. + \frac{1}{4}(-\varphi^{\gamma\gamma'} + \frac{1}{2}\varphi\eta^{\gamma\gamma'})\eta^{\alpha\beta}\eta^{\alpha'\beta'} \right] \partial_\gamma h_{\alpha\beta} \partial_{\gamma'} h_{\alpha'\beta'} \quad (61)
\end{aligned}$$

We also define the rest of the vertex in  $V_g$  as  $V_{g,III}$ :

$$V_{g,III} = \sqrt{-\tilde{g}} \left( h_{\alpha\beta} h_{\gamma\delta} \tilde{R}^{\alpha\gamma\beta\delta} - h_{\alpha\beta} h^\beta{}_\gamma \tilde{R}^{\kappa\alpha\gamma}{}_\kappa - \frac{1}{2} h^{\alpha\beta} h_{\alpha\beta} \tilde{R} \right) \quad (62)$$

The vacuum-to-vacuum amplitudes in the first-layer perturbation can be split into two parts in the second-layer perturbation: the vacuum-to-vacuum amplitudes and the tadpoles.<sup>11</sup> Let us consider the vacuum-to-vacuum amplitudes in the second-layer perturbation. The vacuum energy - which leads to the cosmological constant renormalization - comes from

$$\int \prod_x dh_{\kappa_1\kappa_2} e^{\frac{i}{\kappa^2} \int \left( -\frac{1}{2} \partial_\gamma h^{\alpha\beta} \partial^\gamma h_{\alpha\beta} \right)} \quad (63)$$

One obtains a constant term (see, e.g., the analysis given in [30]) whose divergent part (which will be denoted by  $A_0$  below) is essentially the coefficient of the cosmological constant term. The calculation above leads to a quantum-level cosmological constant. Here is the difference between gravity and a non-gravitational theory. In a non-gravitational theory, appearance of a term absent in the classical action would potentially be a signal toward non-renormalizability.<sup>12</sup> However, in a gravitational theory one has an additional leverage of a metric field redefinition, and we will ponder in section 4.2 the significance of the quantum shift in the cosmological constant in the quantization framework that involves the metric field redefinition.

<sup>11</sup>As we will soon see, there are genuine tadpoles as well, i.e., tadpoles in the first-layer perturbation. As usual we evaluate them through the second-layer perturbation.

<sup>12</sup>Even in a non-gravitational theory, appearance of a *finite* number of new couplings is taken to be compatible with renormalizability.

The evaluation of the vacuum-to-vacuum amplitude, whether it is from the graviton or the ghost (or matter), involves the following integral that is taken to vanish in dimensional regularization:

$$\int d^4p \ln p^2 = 0 \quad (64)$$

Nevertheless, we introduce renormalization by finite renormalization for the following reasons. Although the expression above is taken to vanish in dimensional regularization, the vacuum energy expression (in particular  $A_0$  in (66)) will not, in general, vanish in other regularization methods for a curved background. To better examine the behavior of the integral let us add a mass term  $m^2$  that will be taken to  $m^2 \rightarrow 0$  at the end,

$$\sim \int d^4p \ln(p^2 + m^2) \quad (65)$$

One can then take derivatives with respect to  $m^2$  for its evaluation; the result takes the form of

$$A_f + A_0 + A_1 m^2 + A_2 m^4 \quad (66)$$

where  $A$ 's are some  $m$ -independent constants; the finite piece,  $A_f$ , takes

$$A_f \sim m^4 \ln m^2 \quad (67)$$

With the limit  $m^2 \rightarrow 0$ , only the term with the constant  $A_0$ , which is infinite, survives, and in dimensional regularization one sets  $A_0 = 0$ . Although each term in (66) either vanishes or is taken to zero, not introducing nonvanishing finite pieces seems unnatural (and unlikely to be consistent with the experiment): in a more general procedure of renormalization of a quantum field theory, one can always conduct finite renormalization regardless of the presence of the divergences. (As we will see in section 4.2, not only does the quantum shift need to be introduced but also “classical” piece of the cosmological constant.) Once a finite piece is introduced and the definition of the physical cosmological constant is made (say, as the coefficient of the  $\int \sqrt{-g}$  term), the renormalized coupling will run basically due to the presence of the scale parameter  $\mu$ .

Let us now consider the tadpole diagrams; the tadpole diagrams<sup>13</sup> are responsible for the renormalization of the Newton's constant. For the tadpole, the rest of vertices in the kinetic term in (60) - which are nothing but  $V_{g,II}$  - as well as  $V_{g,III}$  are relevant; the former is part of the vacuum-to-vacuum amplitude in the first-layer perturbation whereas the latter is associated with a genuine tadpole of the first-layer perturbation. It turns out that  $V_{g,II}$  leads to a vanishing result in dimensional regularization; we illustrate that with  $V_{g,I}$ ,

$$V_{g,I} = \left( 2\eta^{\beta\beta'} \tilde{\Gamma}^{\alpha'\gamma\alpha} - \eta^{\alpha\beta} \tilde{\Gamma}^{\alpha'\gamma\beta'} \right) \partial_\gamma h_{\alpha\beta} h_{\alpha'\beta'} \quad (68)$$

The self-contraction of the  $h_{\mu\nu}$ 's in (68) leads to a momentum loop integral with an odd integrand, which thus vanishes. (The other terms in (60) vanish because the self contraction leads to the trace of  $\varphi_{\mu\nu}$ .) The vertex  $V_{g,III}$  similarly leads to a vanishing result. To see this, consider contraction of the  $h_{\alpha\beta}$ -fields in  $V_{g,III}$ . The index structures yield  $R$  but the self-contraction is taken to vanish in dimensional regularization due to the identity in (59). Then for the renormalization of the Newton's constant the story goes similarly to the case of the cosmological constant: although the dimensional regularization does not lead to a divergence for the tadpole diagram, the shift is introduced through finite renormalization.

## 4.2 renormalization by field redefinition

The full one-loop renormalization procedure is in order. Many steps of the procedure below have analogous steps in the Einstein-scalar case studied in [12] and [15]. Presently we put more efforts in keeping track of the finite parts, and comparison with the future experimental results is elucidated in more detail.

Combining all the results so far, the renormalized action plus the counter-

---

<sup>13</sup>Typically, tadpole diagrams in a non-gravitational are cancelled by a counterterm linear in the field and not considered further. More care is needed in a gravitational theory since the counter-terms take the form of the Einstein-Hilbert term. At least a priori it seems safer to view its effect as shifting the Newton's constant. The shift can be set to zero later if, for instance, the consistency of the renormalization program demands its vanishing.

terms are given by

$$\begin{aligned}
& \int \sqrt{-g} (e_1 + e_2 R + e_3 R^2 + e_4 R_{\alpha\beta}^2) \\
& + \int \sqrt{-g} \left( e_5 F_{\mu\kappa} F_{\nu}{}^{\kappa} R^{\mu\nu} + e_6 F_{\alpha\beta} F^{\alpha\beta} R + e_7 F_{\alpha\delta} F_{\beta\gamma} R^{\alpha\beta\gamma\delta} \right. \\
& \left. + e_8 F_{\alpha\beta} F_{\gamma\delta} R^{\alpha\beta\gamma\delta} + e_9 \nabla^\alpha F_{\alpha\kappa} \nabla^\beta F_{\beta}{}^\kappa + e_{10} \nabla_\lambda F_{\mu\nu} \nabla^\lambda F^{\mu\nu} + e_{11} (F_{\alpha\beta} F^{\alpha\beta})^2 + \dots \right)
\end{aligned} \tag{69}$$

where  $e_1$  is the constant previously denoted by  $A_0$ . More precisely,  $[e_1] = A_0$  where the square bracket  $[e_i]$  denotes the infinite parts of the coefficient  $e_i$  calculated by employing dimensional regularization. Similarly, the would-be divergence of the tadpole diagrams will be denoted  $B_0 = [e_2]$ . ( $A_0, B_0$  are taken to vanish in dimensional regularization.) For the rest of the coefficients, one has, by collecting the results in section 3,

$$\begin{aligned}
[e_3] &= -\frac{17}{60} + \frac{23}{80} + \frac{1}{30}, & [e_4] &= -\frac{7}{30} + \frac{23}{40} - \frac{1}{10} - \frac{1}{15}, \\
[e_5] &= \left(-1 + \frac{3}{4}\right) \kappa'^2, & [e_6] &= \frac{\kappa'^2}{8}, & [e_7] &= \frac{\kappa'^2}{4}, & [e_8] &= -\frac{\kappa'^2}{4}, \\
[e_9] &= \frac{\kappa'^2}{6}, & [e_{10}] &= -\frac{\kappa'^2}{24}, & [e_{11}] &= \frac{3}{64} \kappa'^4,
\end{aligned} \tag{70}$$

where the common factor  $\frac{\Gamma(\epsilon)}{(4\pi)^2}$  has been suppressed. The finite pieces of each coefficient are determined by the  $\overline{\text{MS}}$  scheme. Not all these counter-terms are independent because of the following relationships, the second of which is valid up to total derivative terms:

$$\begin{aligned}
F_{\alpha\beta} F_{\gamma\delta} R^{\alpha\beta\gamma\delta} &= \nabla_\mu F_{\nu\rho} \nabla^\mu F^{\nu\rho} + 2F_{\mu\kappa} F_{\nu}{}^{\kappa} R^{\mu\nu} - 2\nabla^\lambda F_{\lambda\kappa} \nabla^\sigma F_{\sigma}{}^\kappa \\
F_{\alpha\delta} F_{\beta\gamma} R^{\alpha\beta\gamma\delta} &= -\frac{1}{2} F_{\alpha\beta} F_{\gamma\delta} R^{\alpha\beta\gamma\delta}
\end{aligned} \tag{71}$$

Upon substituting these into (69), one gets<sup>14</sup>

$$\begin{aligned}
& \int \sqrt{-g} \left[ e_1 + e_2 R + e_3 R^2 + e_4 R_{\alpha\beta}^2 + (e_5 - e_7 + 2e_8) F_{\mu\kappa} F_{\nu}{}^{\kappa} R^{\mu\nu} \right. \\
& \left. + e_6 F_{\alpha\beta} F^{\alpha\beta} R + (e_7 - 2e_8 + e_9) \nabla^\alpha F_{\alpha\kappa} \nabla^\beta F_{\beta}{}^\kappa \right]
\end{aligned} \tag{72}$$

---

<sup>14</sup>The analysis in this section is to illustrate the renormalization procedure and is based on the computation that we have carried out in the previous sections. Some of the diagrams that we did not explicitly calculate will change the numerical values of certain coefficients. For instance, there are tadpole diagrams with the matter fields running on the loop. Such diagrams will generate a counter-term of the form  $\sim F_{\alpha\beta}^2$ .

$$+(-e_7/2 + e_8 + e_{10})\nabla_\lambda F_{\mu\nu}\nabla^\lambda F^{\mu\nu} + e_{11}(F_{\alpha\beta}F^{\alpha\beta})^2 + \dots \Big]$$

The strategy is to absorb these counter-terms by redefining the metric in the bare action. Inspection reveals that the counter-terms of the forms  $\nabla_\lambda F_{\mu\nu}\nabla^\lambda F^{\mu\nu}$ ,  $\nabla^\alpha F_{\alpha\kappa}\nabla^\beta F_\beta^\kappa$  cannot be absorbed by a bare action that consists of the Einstein-Hilbert term and the Maxwell term: one needs the cosmological constant term as well. The reason is that under a metric shift  $g_{\mu\nu} \rightarrow g_{\mu\nu} + \delta g_{\mu\nu}$ , the Einstein-Hilbert part shifts according to

$$\sqrt{-g} R \rightarrow \sqrt{-g} R + R \delta g^{\mu\nu} \frac{\delta\sqrt{-g}}{\delta g_{\mu\nu}} + \sqrt{-g} \delta g^{\mu\nu} \frac{\delta R}{\delta g_{\mu\nu}} \quad (73)$$

so the shifted part comes either with  $R$  or  $R_{\mu\nu}$ , and is thus inadequate to absorb the aforementioned counter-terms; so is the shifted part from the Maxwell's action. We assume the presence of the cosmological constant in the bare action and proceed; more in the conclusion. Let us consider the following shifts<sup>15</sup> [35] [12],

$$\kappa \rightarrow \kappa + \delta\kappa \quad , \quad \Lambda \rightarrow \Lambda + \delta\Lambda$$

$$\begin{aligned} g_{\mu\nu} \rightarrow \mathcal{G}_{\mu\nu} \equiv & l_0 g_{\mu\nu} + l_1 g_{\mu\nu} R + l_2 R_{\mu\nu} + l_3 g_{\mu\nu} F_{\rho\sigma}^2 + l_4 F_{\mu\kappa} F_\nu^\kappa \\ & + l_5 R F_{\mu\kappa} F_\nu^\kappa + l_6 R_{\mu\nu} F_{\kappa_1\kappa_2}^2 + l_7 g_{\mu\nu} R F_{\rho\sigma}^2 + l_8 g_{\mu\nu} R^{\alpha\beta} F_{\alpha\kappa} F_\beta^\kappa \\ & + l_9 R_{\mu\nu}{}^{\alpha\beta} F_{\alpha\kappa} F_\beta^\kappa + l_{10} R (F_{\kappa_1\kappa_2} F^{\kappa_1\kappa_2})^2 \\ & + l_{11} \nabla_\mu F_{\kappa_1\kappa_2} \nabla_\nu F^{\kappa_1\kappa_2} + l_{12} \nabla^\lambda F_{\lambda\mu} \nabla^\kappa F_{\kappa\nu} \end{aligned} \quad (74)$$

One can straightforwardly show that under these, the gravity and matter

---

<sup>15</sup>One may wonder about the traceless condition on the newly defined metric. The traceless condition was in order for the propagator to be well-defined. Once the effective action is obtained, one may choose a different gauge-fixing for solving the field equations in which the traceless condition may not be imposed.

sectors shift, respectively,

$$\begin{aligned}
& -\left(\frac{2}{\kappa^2}\Lambda\right) \int \sqrt{-g} + \frac{1}{\kappa^2} \int d^4x \sqrt{-g} R \rightarrow -2\left(\frac{\Lambda}{\kappa^2} + \frac{\delta\Lambda}{\kappa^2} - \frac{2\delta\kappa\Lambda}{\kappa^3} + 2l_0\Lambda\right) \int \sqrt{-g} \\
& + \left(\frac{1}{\kappa^2} - \frac{2\delta\kappa}{\kappa^3} + \frac{l_0}{\kappa^2} - \frac{\Lambda}{\kappa^2}(4l_1 + l_2)\right) \int \sqrt{-g} R + \frac{1}{\kappa^2} \int \sqrt{-g} \left[ (l_1 + \frac{1}{2}l_2)R^2 - l_2 R_{\mu\nu}R^{\mu\nu} \right] \\
& + \frac{1}{\kappa^2} \int \sqrt{-g} \left[ -\Lambda(4l_3 + l_4)F_{\alpha\beta}F^{\alpha\beta} + \left(l_3 + l_4/2 - \Lambda[l_5 + l_6 + 4l_7]\right)RF_{\alpha\beta}F^{\alpha\beta} \right. \\
& \left. -\Lambda(4l_8 + l_9)R^{\alpha\beta}F_{\alpha\kappa}F_{\beta}{}^{\kappa} - 4\Lambda l_{10}(F_{\rho\sigma}F^{\rho\sigma})^2 - \Lambda l_{11}(\nabla_{\mu}F_{\nu\rho})^2 - \Lambda l_{12}(\nabla^{\kappa}F_{\kappa\nu})^2 + \dots \right]
\end{aligned} \tag{75}$$

and<sup>16</sup>

$$\begin{aligned}
& -\frac{1}{4} \int \sqrt{-g} F_{\mu\nu}^2 \rightarrow -\frac{1}{4} \int \sqrt{-g} F_{\mu\nu}^2 + \int \sqrt{-g} \left[ -\frac{l_2}{8}RF_{\alpha\beta}F^{\alpha\beta} \right. \\
& \left. + \frac{l_2}{2}R^{\alpha\beta}F_{\alpha\kappa}F_{\beta}{}^{\kappa} + \frac{l_3}{2}(F_{\rho\sigma}F^{\rho\sigma})^2 + \frac{l_4}{2}F_{\alpha\kappa}F_{\beta}{}^{\kappa}F^{\alpha\kappa'}F_{\beta}{}^{\kappa'} + \dots \right]
\end{aligned} \tag{76}$$

Combining these two, one gets

$$\begin{aligned}
& \frac{1}{\kappa^2} \int d^4x \sqrt{-g} (R - 2\Lambda) - \frac{1}{4} \int \sqrt{-g} F_{\mu\nu}^2 \rightarrow -2\left(\frac{\Lambda}{\kappa^2} + \frac{\delta\Lambda}{\kappa^2} - \frac{2\delta\kappa\Lambda}{\kappa^3} + 2l_0\Lambda\right) \int \sqrt{-g} \\
& + \left(\frac{1}{\kappa^2} - \frac{2\delta\kappa}{\kappa^3} + \frac{1}{\kappa^2}l_0 - \frac{1}{\kappa^2}\Lambda(4l_1 + l_2)\right) \int \sqrt{-g} R - \frac{1}{4} \int \sqrt{-g} F_{\mu\nu}^2 \\
& + \frac{1}{\kappa^2} \int \sqrt{-g} \left[ (l_1 + \frac{1}{2}l_2)R^2 - l_2 R_{\mu\nu}R^{\mu\nu} \right] + \frac{1}{\kappa^2} \int \sqrt{-g} \left[ -\Lambda(4l_3 + l_4)F_{\alpha\beta}F^{\alpha\beta} \right. \\
& + \left(l_3 + \frac{l_4}{2} - \Lambda[l_5 + l_6 + 4l_7] - \frac{l_2}{8}\kappa^2\right)RF_{\alpha\beta}F^{\alpha\beta} + \left(\kappa^2\frac{l_2}{2} - \Lambda[4l_8 + l_9]\right)R^{\alpha\beta}F_{\alpha\kappa}F_{\beta}{}^{\kappa} \\
& \left. (\kappa^2 l_3/2 - 4\Lambda l_{10})(F_{\rho\sigma}F^{\rho\sigma})^2 - l_{11}(\nabla_{\mu}F_{\nu\rho})^2 - l_{12}(\nabla^{\kappa}F_{\kappa\nu})^2 + \dots \right]
\end{aligned} \tag{77}$$

Not all of the terms in the expansion have not been explicitly recorded: additional diagrams such as 3-pt amplitudes should be considered to account for some of them.

Let us consider the first several coefficients of the shifted action and compare them with those of (72). We start with the cosmological constant term

---

<sup>16</sup>It is likely that the counter-term of the form  $F_{\alpha\kappa}F_{\beta}{}^{\kappa}F^{\alpha\kappa'}F_{\beta}{}^{\kappa'}$  will appear at two-loop.

and Einstein-Hilbert term. Their counter-terms can be absorbed by setting<sup>17</sup>

$$-\frac{2}{\kappa^2} \left( \delta\Lambda - \frac{2\delta\kappa\Lambda}{\kappa} \right) = A_0 \quad (78)$$

and

$$-\frac{2}{\kappa^3} \delta\kappa + \frac{1}{\kappa^2} l_0 - \frac{\Lambda}{\kappa^2} (4l_1 + l_2) = B_0 \quad (79)$$

respectively. We assume that the constants  $A_0, B_0$  now contain the non-vanishing finite pieces introduced by the aforementioned finite renormalization. Eq. (79) determines the infinite part of  $\delta\kappa$

$$\delta\kappa = \frac{\kappa}{2} l_0 - \frac{\kappa\Lambda}{2} (4l_1 + l_2) - \frac{\kappa^3}{2} B_0 \quad (80)$$

$\delta\Lambda$  is determined once this result is substituted into (78):

$$\delta\Lambda = l_0\Lambda - \Lambda^2(4l_1 + l_2) - \frac{\kappa^2}{2} A_0 \quad (81)$$

The counter-terms of the forms  $R^2, R_{\mu\nu}^2$  can be absorbed by setting

$$l_1 + \frac{1}{2} l_2 = e_3 \quad , \quad -l_2 = e_4 \quad (82)$$

which yields

$$l_1 = e_3 + \frac{1}{2} e_4 \quad , \quad l_2 = -e_4 \quad (83)$$

Inspection of the coefficients of  $(F_{\alpha\beta})^2$  implies

$$4l_3 + l_4 = \mathcal{O}(\kappa^4) \quad (84)$$

The coefficients of  $RF_{\alpha\beta}F^{\alpha\beta}, R^{\alpha\beta}F_{\alpha\kappa}F_{\beta}{}^{\kappa}$  should match with the corresponding coefficients of the counter-term action:

$$l_3 + \frac{l_4}{2} - \Lambda(l_5 + l_6 + 4l_7) - \frac{l_2}{8} \kappa^2 = e_6 \quad , \quad \frac{\kappa^2}{2} l_2 - \Lambda(4l_8 + l_9) = e_5 - e_7 + 2e_8$$

These constraints are to be combined with those coming from the higher order counter-terms.

---

<sup>17</sup>Note that  $A_0 = -\mathcal{J}_{div}$  used, e.g., in [12].

### 4.3 scattering predictability and more of 1PI action

It may be useful to recall the case of a non-gravitational theory before considering the gravitational case. Suppose one performed the loop computations and found new vertices required to remove the divergences. In the standard procedure of renormalization, those vertices will be included with the corresponding arbitrary coupling constants in the bare action. If the number of the new vertices is finite, the theory is called renormalizable and one proceeds to obtain the 1PI effective action. If the number is infinite, the theory is declared to be unrenormalizable; the infinite number of coupling constants lead to loss of the predictive power of the theory.

In a gravity theory there are an infinite number of counter-vertices, some of which we have seen in section 3. The idea of the field redefinition is that one starts with the bare action of the same form as the classical action with possible addition of the cosmological constant term. The metric in the bare action is the field-redefined one,  $\mathcal{G}_{\mu\nu}$ , in (74). The crucial point is that all of the coupling constants associated with the higher-order counter-vertices are absorbed into the *redefined* metric  $\mathcal{G}_{\mu\nu}$ , thus unobservable [35]. The predictability of the theory for scattering amplitudes then follows. Let us paraphrase. The divergences arising from the loop diagrams can be removed by the counter-vertices present on the right-hand side of the definition of  $\mathcal{G}_{\mu\nu}$  in (74). In other words, with the counter-terms added, the renormalized action now contains all of the new coupling constants. However, the counter-terms with those coupling constants can be combined into Einstein-Hilbert form in terms of the redefined metric  $\mathcal{G}_{\mu\nu}$ . This means that the bare action has two coupling constants, the cosmological and Newton's, in terms of the new metric, and therefore the theory is predictive.

More specifically, the theory becomes predictive by following the usual “routines”: suppose the experimental values of the cosmological and Newton's constants are known accurately to the extent that we may discern the quantum corrections. One can find the values of the renormalized cosmological and Newton's constants by imposing certain renormalization conditions. Once the renormalized constants are determined in terms of physical constants one can proceed to compute, for instance, various scattering amplitudes and make predictions on the corresponding experimental outcomes.

The fact that the infinite number of the coupling constants are absorbed by the metric field redefinition must be not taken as to mean that the quantum

effects are immaterial. There will be all those vertices present with fixed finite values of the coefficients in the effective action.<sup>18</sup> At this point one can consider yet another field redefinition in conjunction with the quantum deformation of the geometry that plays an important role in the context of black hole information [36] [19] [16].

## 5 Conclusion

In this work, we have extended the one-loop renormalization of an Einstein-scalar system to an Einstein-Maxwell system. As in the previous works the amplitude calculations have been carried out with the two layers of perturbation in the refined background field method. Since the Maxwell part itself is a gauge system, the extension involves overcoming several additional hurdles. The direct Feynman diagrammatic computation has led to a gauge choice-dependent 1PI effective action: the effective action is covariant only up to the metric gauge-fixing. The origin of the dependence was found in the limitation of the background field method. The proper interpretation of the gauge-choice independence is such that the effective action is made covariant by removing all of the terms containing the gauge-fixing condition. At the same time, the action is to be supplemented by the gauge-fixing condition in the usual manner. We have taken one step further compared to our previous works: with the fixed renormalization scheme chosen, we have enumerated the quantum corrections of various physical quantities such as the cosmological and Newton's constants. The role of the finite renormalization is important. We have seen that the metric field redefinition a la 't Hooft brings predictive power to the theory.

There are several highlights worth recapitulating. Firstly, note that one ends up taking three different measures to ensure the covariance: removal of the trace part of the metric, employment of the refined BFM, and enforcement of the strong form of the gauge-fixing. Secondly, the cosmological constant has several special features in the context of renormalization. It is the leading term in the derivative expansion and generically generated regardless of the background under consideration. Even if one's starting ac-

---

<sup>18</sup>In general a full effective action is a highly complicated object even containing nonlocal terms (that may be important for the black hole physics [37]). Here we focus on the starting renormalized action with the added vertices with the fixed finite coefficients.

tion does not include the cosmological constant term, the renormalizability dictates its presence in the bare action (and thus in the effective action). Thirdly, the renormalizability requires a metric field definition. The existence of such a field redefinition should not be a coincidence but must be a reflection of the quantum deformation of the geometry. The freedom of such a field redefinition is powerful and distinguishes gravity from non-gravitational unrenormalizable theories.

We have seen that the renormalizability requires the presence of the cosmological term in the bare action. One may take this as a rationale of the presence of a renormalized cosmological constant in the starting renormalized action. In fact, this seems to suggest a future direction that stands out. In the main body we carried out the analysis without including the cosmological constant since we were interested in a flat background. The fact that the cosmological constant is generically generated and required for the renormalizability seems to suggest the possibility that it should be included in the starting renormalized action. This would imply that one should consider the propagator associated with a de Sitter (or anti-de Sitter) background, although the flat spacetime analysis can still be employed for the divergence analysis. Once the cosmological constant is included and expanded around the fluctuation metric, it can be treated as a source for additional vertices.<sup>19</sup>

It appears that there are several variant renormalization procedures depending on, e.g., whether or not to include the cosmological constant in the starting renormalized action. As a matter of fact, there is an intriguing possibility when choosing a renormalization scheme. Although the flat space analysis catches the divergent parts of the proper curved space analysis, the finite parts require, in general, the due curved space propagators. One may choose the renormalization scheme such that the finite parts become the same as the corresponding flat analysis. It will be interesting to see whether or not the renormalization procedure could be consistently conducted with such a special scheme. If it could be and yields the same results as the curved space analysis, the flat space analysis will serve as a highly convenient alternative

---

<sup>19</sup>Alternatively, it can be treated as the “graviton mass” term and with this the graviton propagator becomes a massive one. This may appear too contrived but the massive propagator makes it unnecessary to introduce the finite renormalization. An objection may be raised that the spacetime is no longer flat in the presence of the cosmological constant term. This is an issue worth further exploring. The bottom line is that the flat space analysis catches the divergences. Also, in a more realistic setup including a Higgs-type scalar, mixing between the physical and unphysical states [38] is expected.

to the proper curved space analysis, and that would imply, in a certain sense, the background independence of the whole framework.

Another direction is the two-loop extension of the results of the present work. As stated in the introduction, the renormalization procedure in this paper is entirely within the standard framework and in particular the reduction of the physical states did not play a role (other than providing assurance that the present procedure can, in principle, be extended to two- and higher-loops. Although the direct two-loop analysis is expected to be much harder, the difficulty will be of technical character and associated with computing the Feynman diagrams themselves. One may turn to the approach where the counter-terms are determined by dimensional analysis and covariance [39]. Once the counter-terms are obtained one way or another, it should be possible, with reasonable effort, to extend the field redefinition-utilized renormalization to two-loop. The reduction to the physical sector [7, 11] is expected to play a role at two- and higher- loops.

## References

- [1] N. D. Birrell and P. C. W. Davies, “Quantum Fields in Curved Space,” Cambridge University Press (1982)
- [2] A. O. Barvinsky and G. A. Vilkovisky, “The Generalized Schwinger-Dewitt Technique in Gauge Theories and Quantum Gravity,” Phys. Rept. **119**, 1 (1985). doi:10.1016/0370-1573(85)90148-6
- [3] I. L. Buchbinder, S. D. Odintsov and I. L. Shapiro, “Effective action in quantum gravity,” IOP Publishing (1992)
- [4] V. P. Frolov and I. D. Novikov, “Black Hole Physics: Basic Concepts and New Developments,” Springer (1998)
- [5] J. F. Donoghue, “General relativity as an effective field theory: The leading quantum corrections,” Phys. Rev. D **50**, 3874 (1994) doi:10.1103/PhysRevD.50.3874 [gr-qc/9405057].
- [6] V. F. Mukhanov and S. Winitzki, “Introduction to quantum effects in gravity” Cambridge (2007)
- [7] I. Y. Park, “Hypersurface foliation approach to renormalization of ADM formulation of gravity,” Eur. Phys. J. C **75**, no. 9, 459 (2015) doi:10.1140/epjc/s10052-015-3660-x [arXiv:1404.5066 [hep-th]]; “Quantization of gravity through hypersurface foliation,” arXiv:1406.0753 [gr-qc], to appear in ATMP; “Foliation, jet bundle and quantization of Einstein gravity,” Front. in Phys. **4**, 25 (2016) doi:10.3389/fphy.2016.00025 [arXiv:1503.02015 [hep-th]].
- [8] I. Y. Park, “Lagrangian constraints and renormalization of 4D gravity,” JHEP **1504**, 053 (2015) doi:10.1007/JHEP04(2015)053 [arXiv:1412.1528 [hep-th]].
- [9] I. Y. Park, “4D covariance of holographic quantization of Einstein gravity,” Theor. Math. Phys. **195**, 745 (2018) doi:10.1134/S0040577918050094 [arXiv:1506.08383 [hep-th]].
- [10] I. Y. Park, “Holographic quantization of gravity in a black hole background,” J. Math. Phys. **57**, no. 2, 022305 (2016) doi:10.1063/1.4942101 [arXiv:1508.03874 [hep-th]].

- [11] I. Y. Park, “Reduction of gravity-matter and dS gravity to hypersurface,” *Int. J. Geom. Meth. Mod. Phys.* **14**, no. 06, 1750092 (2017) doi:10.1142/S021988781750092X [arXiv:1512.08060 [hep-th]].
- [12] I. Y. Park, “One-loop renormalization of a gravity-scalar system,” *Eur. Phys. J. C* **77**, no. 5, 337 (2017) doi:10.1140/epjc/s10052-017-4896-4 [arXiv:1606.08384 [hep-th]]
- [13] I. Y. Park, “ADM reduction of Einstein action and black hole entropy,” *Fortsch. Phys.* **62**, 950 (2014) doi:10.1002/prop.201400056 [arXiv:1304.0014 [hep-th]].
- [14] I. Y. Park, “Quantum “violation” of Dirichlet boundary condition,” *Phys. Lett. B* **765**, 260 (2017) doi:10.1016/j.physletb.2016.12.026 [arXiv:1609.06251 [hep-th]].
- [15] F. James and I. Y. Park, “Quantum gravitational effects on boundary,” *Theor. Math. Phys.* **195**, 605 (2018) doi:10.1134/S0040577918040116 [arXiv:1610.06464 [hep-th]].
- [16] A. J. Nurmagambetov and I. Y. Park, “Quantum-induced trans-Planckian energy near horizon,” *JHEP* **1805**, 167 (2018) doi:10.1007/JHEP05(2018)167 [arXiv:1804.02314 [hep-th]].
- [17] E. Witten, “A Note On Boundary Conditions In Euclidean Gravity,” arXiv:1805.11559 [hep-th].
- [18] F. James and I. Y. Park, “On the pattern of black hole information release,” *Int. J. Mod. Phys. A* **29**, 1450047 (2014) doi:10.1142/S0217751X1450047X [arXiv:1301.6320 [hep-th]].
- [19] I. Y. Park, “Foliation-based quantization and black hole information,” *Class. Quant. Grav.* **34**, no. 24, 245005 (2017) doi:10.1088/1361-6382/aa9602 [arXiv:1707.04803 [hep-th]].
- [20] S. Deser and P. van Nieuwenhuizen, “One Loop Divergences of Quantized Einstein-Maxwell Fields,” *Phys. Rev. D* **10**, 401 (1974). doi:10.1103/PhysRevD.10.401
- [21] G. A. Vilkovisky, “The Unique Effective Action in Quantum Field Theory,” *Nucl. Phys. B* **234**, 125 (1984). doi:10.1016/0550-3213(84)90228-1

- [22] E. S. Fradkin and A. A. Tseytlin, “On the New Definition of Off-shell Effective Action,” Nucl. Phys. B **234**, 509 (1984). doi:10.1016/0550-3213(84)90075-0
- [23] S. R. Huggins, G. Kunstatter, H. P. Leivo and D. J. Toms, “The Vilkovisky-de Witt Effective Action for Quantum Gravity,” Nucl. Phys. B **301**, 627 (1988). doi:10.1016/0550-3213(88)90280-5
- [24] S. D. Odintsov, “The Parametrization Invariant and Gauge Invariant Effective Actions in Quantum Field Theory,” Fortsch. Phys. **38**, 371 (1990); “Vilkovisky effective action in quantum gravity with matter,” Theor. Math. Phys. **82**, 45 (1990) [Teor. Mat. Fiz. **82**, 66 (1990)]. doi:10.1007/BF01028251.
- [25] S. D. Odintsov and I. N. Shevchenko, “Gauge invariant and gauge fixing independent effective action in one loop quantum gravity,” Fortsch. Phys. **41**, 719 (1993) [Yad. Fiz. **55**, 1136 (1992)] [Sov. J. Nucl. Phys. **55**].
- [26] R. E. Kallosh, O. V. Tarasov and I. V. Tyutin, “One Loop Finiteness Of Quantum Gravity Off Mass Shell,” Nucl. Phys. B **137**, 145 (1978). doi:10.1016/0550-3213(78)90055-X
- [27] D. M. Capper, J. J. Dulwich and M. Ramon Medrano, “The Background Field Method for Quantum Gravity at Two Loops,” Nucl. Phys. B **254**, 737 (1985). doi:10.1016/0550-3213(85)90243-3
- [28] I. Antoniadis, J. Iliopoulos and T. N. Tomaras, “One loop effective action around de Sitter space,” Nucl. Phys. B **462**, 437 (1996) doi:10.1016/0550-3213(95)00633-8 [hep-th/9510112].
- [29] T. R. Morris, “Quantum gravity, renormalizability and diffeomorphism invariance,” arXiv:1806.02206 [hep-th].
- [30] S. Weinberg, “The quantum theory of fields”, vol II, Cambridge university press (1995)
- [31] G. Sterman, “An introduction to quantum field theory”, Cambridge university press (1993)

- [32] M. Reuter, “Nonperturbative evolution equation for quantum gravity,” *Phys. Rev. D* **57**, 971 (1998) doi:10.1103/PhysRevD.57.971 [hep-th/9605030].
- [33] I. Donkin and J. M. Pawłowski, “The phase diagram of quantum gravity from diffeomorphism-invariant RG-flows,” arXiv:1203.4207 [hep-th].
- [34] K. Falls, “Renormalization of Newton’s constant,” *Phys. Rev. D* **92**, no. 12, 124057 (2015) doi:10.1103/PhysRevD.92.124057 [arXiv:1501.05331 [hep-th]].
- [35] G. ’t Hooft, “An algorithm for the poles at dimension four in the dimensional regularization procedure,” *Nucl. Phys. B* **62**, 444 (1973). doi:10.1016/0550-3213(73)90263-0
- [36] I. Y. Park, “Quantum-corrected Geometry of Horizon Vicinity,” *Fortsch. Phys.* **65**, no. 12, 1700038 (2017) doi:10.1002/prop.201700038 [arXiv:1704.04685 [hep-th]].
- [37] V. F. Mukhanov, A. Wipf and A. Zelnikov, “On 4-D Hawking radiation from effective action,” *Phys. Lett. B* **332**, 283 (1994) doi:10.1016/0370-2693(94)91255-6 [hep-th/9403018].
- [38] R. Pius, A. Rudra and A. Sen, “Mass Renormalization in String Theory: General States,” *JHEP* **1407**, 062 (2014) doi:10.1007/JHEP07(2014)062 [arXiv:1401.7014 [hep-th]].
- [39] M. H. Goroff and A. Sagnotti, “The Ultraviolet Behavior of Einstein Gravity,” *Nucl. Phys. B* **266**, 709 (1986).